Types of filamentation in tapered diode amplifiers: their causes and features

Elhanan Pniel [1], Benjamin Dalin [1], Sveta Golod [2], Shlomo Goldin [1, 2] * and Eyal Shekel [2] #

[1] *Applied Physics Department, Jerusalem College of Technology, 21 Havaad Haleumi, Jerusalem 9372115, Israel*

[2] *Civan Advanced Technologies Ltd., 64 Kanfei Nesharim, Jerusalem 9546455, Israel*

(*corresponding authors' E-mails:* * shlomog@jct.ac.il # eshekel@civan.co.il)

Abstract. Software for calculation of gain-current relation, gain saturation, light-induced refractive index change and light propagation in diode amplifiers and lasers is developed. Three orders of filamentation are found in tapered (flared) amplifiers within the typical ranges of the parameters. While the 1st order is caused by small external perturbations, the 2nd and 3rd orders are generated by the optical beam itself. The causes of the different types of filamentation are elucidated and their dependence on the amplifier geometry is investigated. Practical guidelines for filamentation suppression are suggested.

Key words: Filamentation; Tapered power amplifiers; Diode lasers; High-brightness; Simulation software.

1. Introduction

High-brightness diode lasers and amplifiers are desirable for many applications, such as molecular spectroscopy, fiber-optic and free-space telecommunications, laser display technology, nonlinear frequency conversion, medical treatments, material processing and fiber-laser pumping. It was found over 20 years ago that tapered (flared) geometries favor filamentation suppression [Walpole 1992; Mehuys 1992]. However, filamentation still remains the main obstacle for the achievement of higher power with high-brightness, even in this type of devices. A significant effort has been made to find structures and geometries where filamentation is less pronounced. Some works [Bossert 1997; Dente 2001; Mikulla 2000; Paxton 1991; Sumph 2009] concentrated on the epitaxial layers structure while many others focused on the lateral geometry [Borruel 2004, 2008; Delépine 2001; Lang 1993; Walpole 2000; White 1995a; Tijero 2014]. In fact, two different filamentation scenarios were considered. In one of them, the filaments were ignited by a small initial perturbation (which can be always assumed to be present in a real structure) [Bossert 1997; Dente 2001; Lang 1993; Paxton 1991]. In the other scenario, they developed as side-lobes of the main light beam [Borruel 2004b, 2008; White 1995]. In this work, it is found, in particular, that these two different scenarios correspond to two different types of filamentation. The filaments of these two types have different origins; they appear at different stages of light propagation and in different fashions.

In the next section of this paper, the software we developed and used to investigate filamentation is briefly described. Section 3 is devoted to the results. The filamentation dependence on the main geometrical parameters of an amplifier is presented. The reasons for different types of filamentation are explained and practical recommendations on how to avoid them are given. The paper is concluded with a short summary.

2. Numerical methods

In this work, a common separate confinement heterostructure is considered. Electronic states are calculated using the transfer matrices approach adjusted to the solution of the Schrodinger equation instead of the wave equation, which allows us to treat arbitrary layer structures.

Material gain is first determined using standard formulas [Coldren 1995, Chinn 1988] as a function of quasi-Fermi-levels separation:

$$g(E) = \frac{\pi e^2 \hbar}{\varepsilon_0 c m_e^2} \frac{|M|^2}{E n_{WG}} \sum_{i,j} C_{ij}^2 A_{ij} \rho_{ij}(E)[f_c + f_v - 1] \quad (1)$$

where M is the transfer matrix element related to atomic wavefunctions, E is the photon energy, n_{WG} is the refractive index in the waveguide, C_{ij} is the electron-hole wavefunction overlap, $\rho_{ij}(E)$ is the electron-hole pair reduced density of states, A_{ij} is an anisotropy factor [Chinn 1988] and $f_{c(v)}(E_{e(h)}, \mu_{e(h)})$ are electron (hole) Fermi functions while $\mu_{e(h)}$ are electron (hole) quasi-Fermi-levels.

The summation is over different electron and hole subbands. Since the optical waveguide is wide compared to the electronic wavelength, we separate the electronic states into 2D subbands in the quantum well and a 3D continuum in the waveguide. In the latter, the summation is then replaced by integration over energies; that highly speeds up the calculation. In order to take into account intraband relaxation, the formula (1) is convolved with a lineshape broadening function:

$$g_{material}(E) = \int_0^\infty g(E_0) L(E - E_0) dE_0 \quad (2)$$

where $L(E)$ is the Fourier transform of $\exp(-L(t))$ while $L(t)$ is given by the formula [Chinn 1988, Coldren 1995]:

$$\log_{10} L(t) = 2 + 1.5\log_{10} t - 0.5\sqrt{(2 + \log_{10} t)^2} + 0.36 \quad (3)$$

In addition, gain spectrum shift caused by bandgap renormalization is considered. Modal gain is obtained through the multiplication of $g_{material}$ by the factor of the optical mode overlap with the quantum well.

Inter-band (conduction to valence band transitions) contribution to the carrier-induced refractive index change is found through Kramers-Kronig relations using formula (1) that leads to,

$$\Delta\varepsilon_r^{inter}(\omega) = -\frac{2e^2\hbar^2|M|^2}{\varepsilon_0 m_e^2} \int_0^\infty \sum_{i,j} C_{ij}^2 A_{ij} \rho_{ij}(E)[f_c + f_v - 1] \frac{E - \hbar\omega}{E(E + \hbar\omega)\left[(E - \hbar\omega)^2 + \left(\frac{\Gamma}{2}\right)^2\right]} dE \quad (4)$$

Here, the intraband relaxation is represented by Lorenzian broadening. Intra-band contributions can be approximated to a good accuracy [Wenzel 1999] by the familiar Drude formula.

As well as the gain and the refractive-index change mentioned above, current is also calculated as a function of the quasi-Fermi-levels separation. Spontaneous emission, leakage and Auger contributions to the current are taken into account as described in Ref. [Coldren 1995, Chinn 1988]. Stimulated-emission contribution is calculated as a function of the quasi-Fermi-levels separation and the optical power density:

$$J_{st} = e g_{modal} P_x / \hbar\omega \quad (5)$$

where g_{modal} is the modal gain, while P_x is the optical power per unit width of the structure. Specification of the total current density then yields the quasi-Fermi-levels separation as an implicit function of the light intensity. This allows calculating the gain saturation and the refractive-index change induced by light. We used a look-up table and interpolation to invert the implicit function, significantly reducing the computation time.

The propagation of light throughout the amplifier is treated using a well-known effective-index approximation (e.g. see [Coldren 1995]). Namely, the optical modes in the vertical (z in Fig. (1)) direction are calculated using the transfer-matrix method. Their effective index in every (x,y)-point is then considered as the refractive index for the simulation of a 2D propagation in the (x,y)-plane. The latter is worked out using the Crank-Nicolson finite-difference Beam Propagation Method.

Although our methods and software can be used for both amplifiers and lasers (lasers can be simulated by sequential back and forth propagations until a convergence is achieved), in the following

we consider only a single-pass amplifier whose geometry is shown in Fig. 1. The amplifier consists of a ridge waveguide (whose role is to filter higher modes leaving a single mode) and a taper whose width increases in the propagation direction (most of the amplification occurs in the taper). The ranges of the device parameters investigated in this work are displayed in Table 1. In order to focus on the physics of the filamentation in the taper and keep away any effects caused by a possible poor filtering in the ridge, we seeded the amplifier with a beam whose shape fitted the optical mode of the ridge waveguide (without current). The total power of the seed was 50 mW .

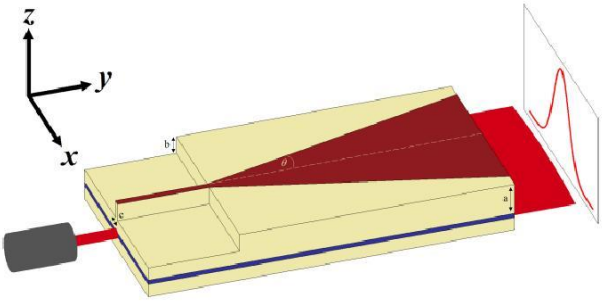

Fig. 1. Schematic diagram of the device. In dark red: p-electrode. θ is the half taper angle. a, b and c are the ridge height, etching depth, and ridge width (respectively). The ridge height, a constant value, is measured from the core to the top of the ridge.

	Minimal	Typical	Maximal
Half taper angle	1°	2°	7.5°
Current density	0	1250 A/cm^2	5000 A/cm^2
Etching depth	0.91 µm	1.03 µm	1.1 µm
Ridge height	-	1.1 µm	-
Ridge width	2 µm	3 µm	4 µm
Ridge length	-	725 µm	-
Wavelength	-	0.976 µm	-
Device length	3500 µm	4300 µm	20000 µm
Device width	603 µm	603 µm	1703 µm

Table 1. The ranges of values, including the typical values, of the investigated parameters of the device.

3. Results

Three orders of filamentation have been observed in this work: 1st, 2nd and 3rd (see Fig. 2). As described hereafter, these orders appear at different stages of light propagation and in different ways. Moreover, they have very different dependences on the amplifier geometry. 2nd and 3rd orders are sometimes called “bat ears” [White 1995b]. In Fig. 2, filaments of all three orders are small and can be seen together. This is a very special situation; usually, one of them becomes dominant, consumes much of the optical power and destroys the beam shape.

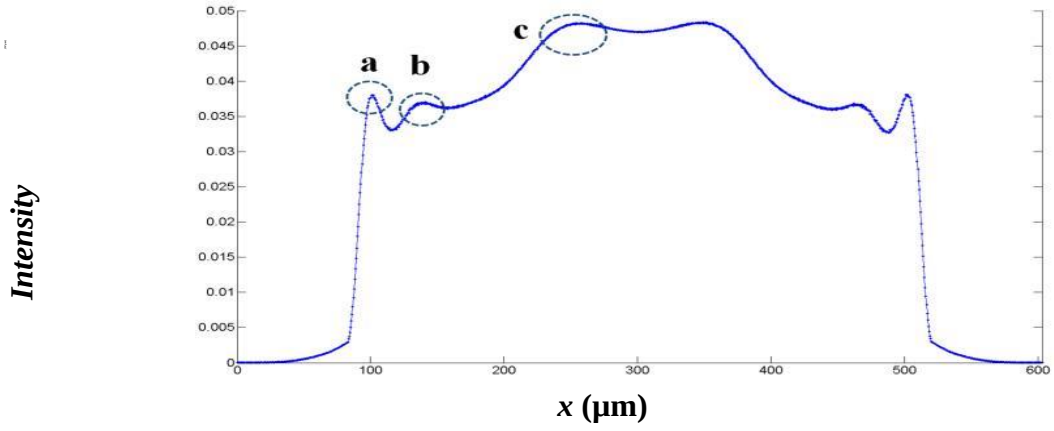

Fig. 2. Three types of filamentation are visible: a, b and c are 1st order, 2nd order and 3rd order filaments (respectively).

First order filaments originate near the beginning of the taper region, though not necessarily within the taper itself. As seen from Fig. 3a, which shows their trajectories in the (xy)-plane, they propagate in straight lines at certain angles. Generally, many filaments of the 1st order may be present. As seen from Figs. 3b-3d, the filament angles are independent of current density, half taper

angle and etching depth. Closer inspection of these filaments' appearance reveals that they originate from an extremely small perturbation. This is a kind of filamentation considered in Ref. [Bossert 1997; Dente 2001; Paxton 1991] where it was found that the filaments grow exponentially. The triggering small perturbations can originate from current or thermal fluctuations which are almost unavoidable. Poor filtering in the ridge section may also lead to this kind of filaments [Sujecki 2003]. Interestingly, in our work they were actually caused by the ridge. This can be noticed from Fig. 4a which shows the Fourier transform of the electric field at the ridge output (in the beginning of the taper). It reveals intensity ripples at the angles close to the filament angles in Fig. 3a. Moreover, if this beam is allowed to propagate in a homogenous non-amplifying space, the ripples, akin to the filaments, advance in straight lines (see Fig. 4b). However, the angles are somewhat different from the filament angles. Furthermore, the ripple angles increase with the decreasing etching depth (up to 40% in the investigated range of parameters), contrary to the filament angles. We notice that the ripples do not appear if there is no current in the ridge, i.e. they are themselves a result of nonlinear light propagation. In any case, the crucial point in the formation of the 1st order filaments is that there exists an unnecessary amplifying medium which lets the initial perturbation grow. In the present simulations, the free diffraction angle of the beam is frequently less than the minimal filament angle. The 1st order filaments then find an amplifying medium unoccupied by useful light between the free diffraction angle and the taper angle. This is consistent with the observations [Borruel 2008; Delépine 2001] that the taper angle should be close to the free diffraction angle.

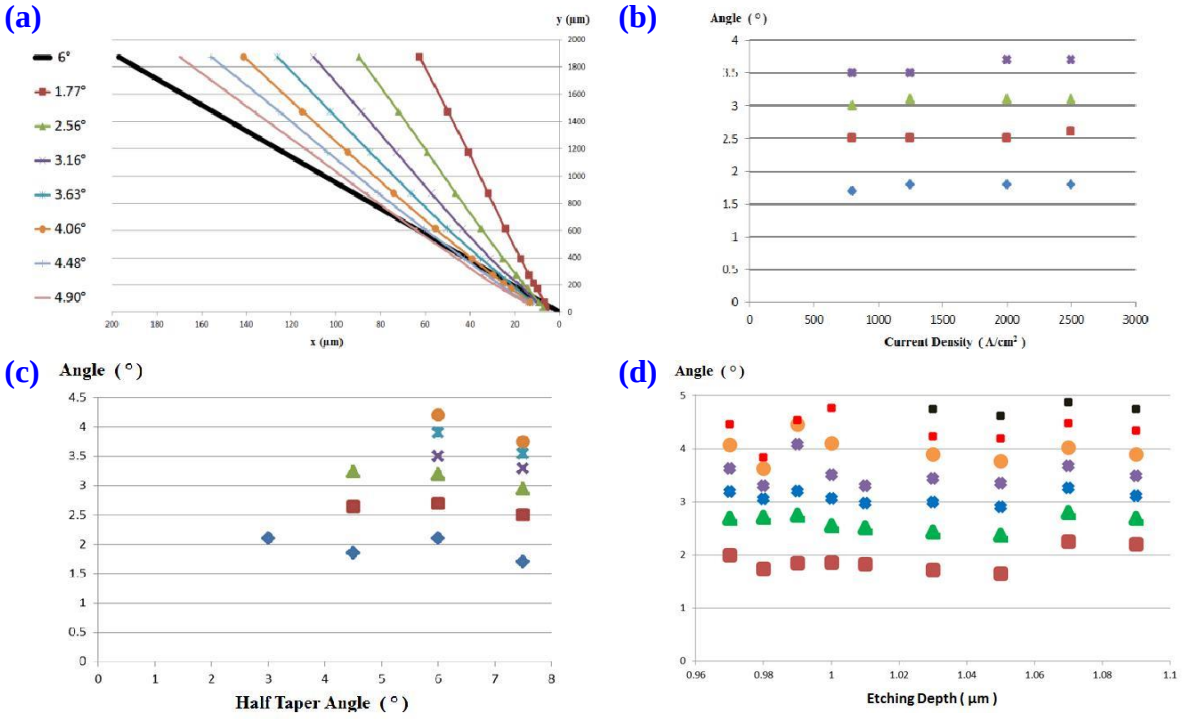

Fig. 3. (a) Propagation of 1st order filaments in the left half of the taper. The thick black line indicates the taper edge. Each of the other lines represents the position of a filament. The filaments originate outside the taper and propagate linearly. (b), (c), (d) 1st order filament angles as functions of current density (b), the half taper angle (c) and the etching depth (d). Unless otherwise specified, the parameter values in all figures are the "typical" ones mentioned in Table 1. The half taper angle is 6° (except for fig. (c)). For wide taper angles in fig. (c), the device width is larger than the typical one.

A natural solution to the problem of the 1st order filaments is the choice of a (half) taper angle below the minimal filament angle. We notice that it is not sufficient to match between the taper angle

and the free diffraction angle. Namely, if both the taper and the free diffraction angles are large, these filaments may sometimes overcome the main beam.

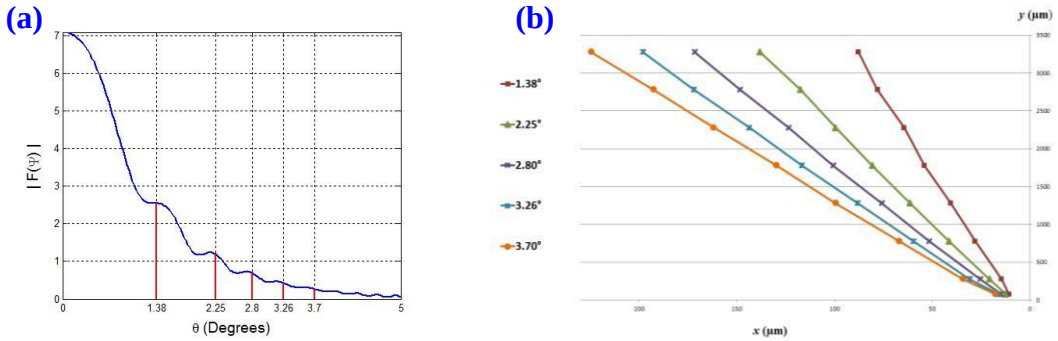

Fig. 4. (a) The Fourier transform of the electric field distribution at the ridge output (a.u.), (b) the ripples in the intensity distribution propagating in a homogenous non-amplifying space. The parameters are the same as in Fig. 3a, except that, in fig. (b), there is no current in the taper section.

Second order filaments propagate at smaller angles than first order filaments, and rarely form when first order filaments are present. As can be seen from the series of images shown in Fig. 5a, they start to form in the middle of the propagation through the taper as a kind of "shoulders" in the intensity distribution (this type of filaments was observed in Ref. [Sujecki 2003; White 1995b]). Fig. 6a shows that they originate near the taper edge and that their angles of propagation are close to the taper angle. Fig. 6b reveals their lack of dependence on the etching depth, while Fig. 6c exhibits their slight dependence on the current density. All these results indicate that 2nd order filaments are caused by the taper edge. This is further proved by consideration of the taper edge "smoothing", i.e. gradually reducing the current density at the edge of the taper in a linear fashion from its maximum to zero. Fig. 6d demonstrates that such a smoothing can almost entirely eliminate the 2nd order filaments. In contrast, we observed that 1st order filaments are not influenced by taper edge smoothing. This is because their origin is unrelated to the taper edge.

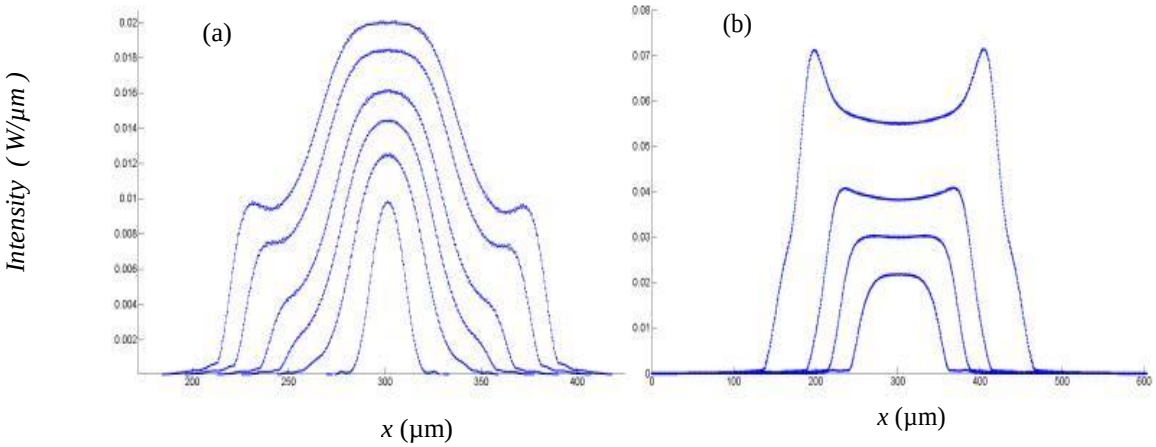

Fig. 5. (a) 2nd order filaments at the beginning of their development. The images are taken at the distances 500, 1000, 1275, 1500, 1800 and 2000 μm from the beginning of the taper. The half taper angle here is 2°. The filaments emerge as "shoulders" in the intensity distribution around its middle value. (b) Top-hat intensity distribution (two lower curves: y = 3000 and 4000 μm) leads to the formation of 3rd order filaments (two higher curves: y = 5000 and 7000 μm). The half taper angle here is 1.5°. Except for the taper angle and the device length, the parameter values in both figures are the "typical" ones mentioned in Table 1.

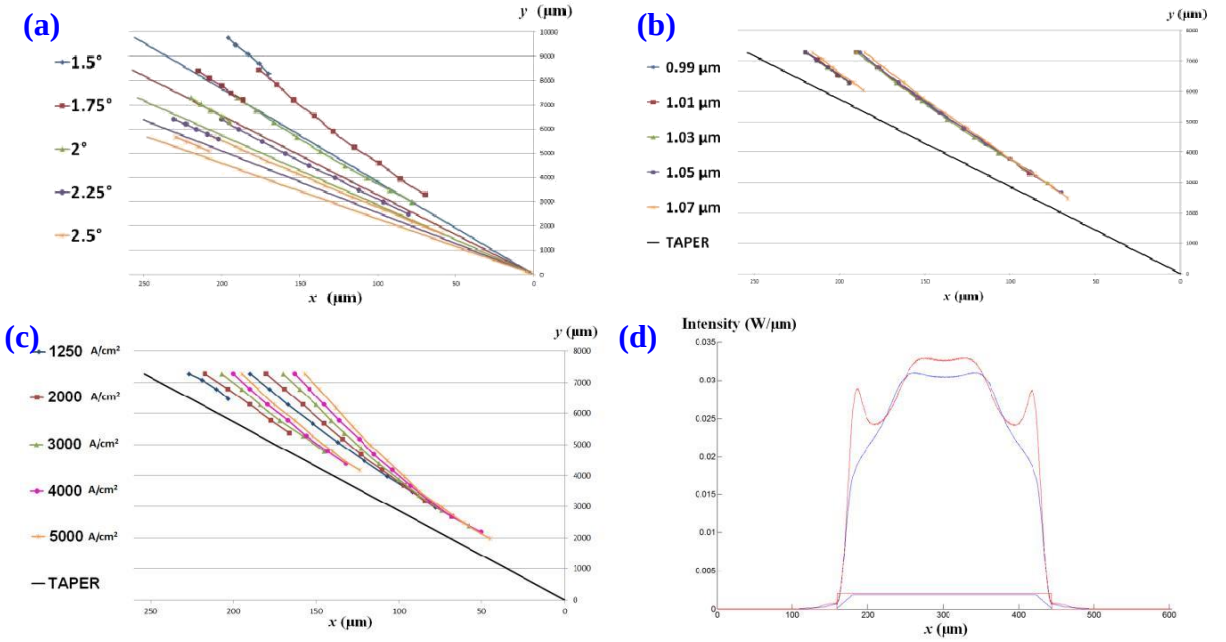

Fig. 6. (a) Propagation of 2nd order filaments in the left half of the taper at different taper angles. The smooth lines indicate the taper edge at different half taper angles, while the dotted lines show the corresponding filament trajectories. Two filaments are present for each value of the taper angle ; (b) The filament trajectories as a function of the etching depth (in different colors). The black line indicates the taper edge; (c) The filament trajectories as functions of the current density. The black line indicates the taper edge; (d) Intensity distribution profile at the front facet with a sharp (red) and with a smoothed (blue) current profiles. The current profiles are indicated at the bottom. The half taper angle here is 2.25°. Unless otherwise specified, the parameter values in all figures are the "typical" ones mentioned in Table 1 (except for the device length, which can be derived from the pictures).

The reasons for the 2nd order filaments' formation and the mechanism of their elimination by current profile smoothing are revealed in Figs. 7a and 7b. Sharpness of the taper edge leads to a mismatch between the optical intensity which is depleted near the taper edge and the current density which remains constant. This leads to a large gain peak near the taper edge (charge carriers gathering in this region was already noticed in Ref. [Borruel 2004b, 2008; Sujecki 2003; White 1995b]). The photons generated there are drawn towards the center of the beam by a refractive index variation. This self-focusing is, in fact, a useful process because it helps to maintain a desired beam shape where the majority of the optical power is located near the center (though under different conditions it can become destructive [Tijero 2014]). The problem arises when the photon flow is slowed down and they begin to pile up somewhere (in Fig. 7a it happens around $x = 230\ \mu m$). The pile first appears as a "shoulder" in the intensity distribution. This flat "shoulder" leads to flatness in the graph of the refractive index. In the absence of a refractive index variation, the drift of photons towards the center stops. The photons arriving from the edge continue to pile up and a filament rapidly develops. Smoothing the edge of the taper significantly reduces the gain in its vicinity (Fig. 7b). As a result, fewer photons are generated there and, consequently, less flow towards the center. More importantly, however, a close inspection of Fig. 7b reveals that the refractive index variation in the problematic region $x = 220 - 240\ \mu m$ is significantly larger there than in Fig. 7a, so the photons do not get stuck. Fewer photons arrive, they are better drawn out and the filament development is significantly suppressed.

We notice that the mechanism of the 2nd order filaments' launching by the taper edge is very different from the one proposed in Ref. [White 1995a] and presumed in Ref. [White 1995b]. These filaments do not evolve from an intensity perturbation caused by the taper edge. They originate at a

significant distance ($x = 20 - 30\ \mu m$) from the edge. The meaning of smoothing is not in the reduction of the first and the second derivatives causing the perturbation as supposed in Ref. [White 1995a], but rather in the mitigation of the imbalance between the current density profile (and a consequent gain profile) and the optical intensity profile.

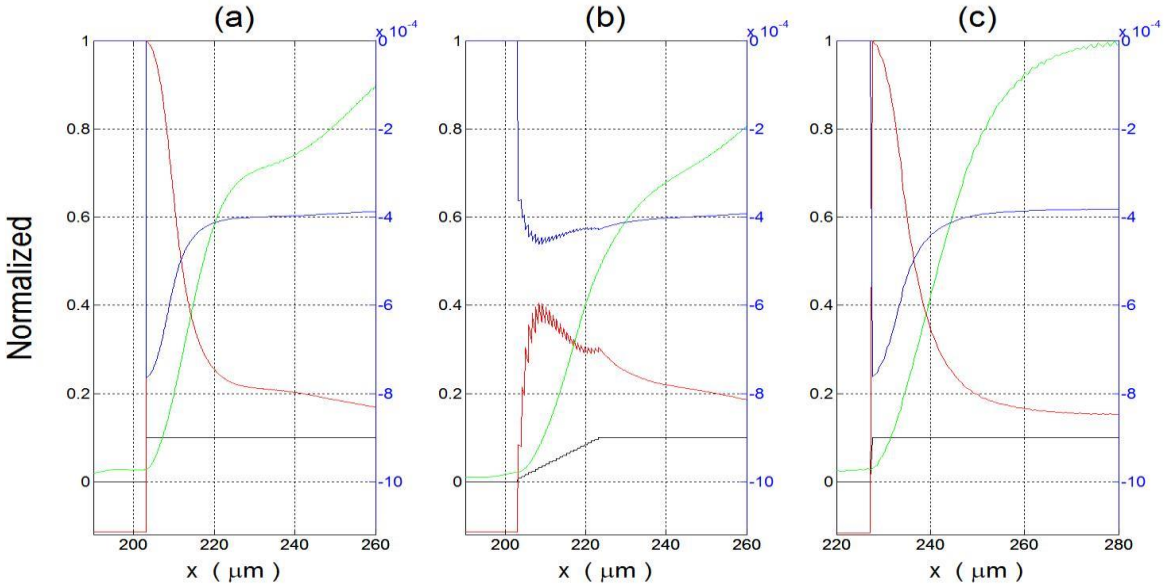

Fig. 7. Normalized light intensity (green), normalized gain (red) – both on the left scale, refractive index change (blue) – right scale, and current density (black, a.u.) for: (a) a device with sharp taper edge (the half taper angle is 2°), (b) a device with smoothed current profile (the same half taper angle; light intensity and gain normalized to the same values as in (a)), and (c) a device with half taper angle of 1.5° (sharp taper edge). The images are taken at $y = 3500\ \mu m$. The taper center is at $x = 301.5\ \mu m$. Unless otherwise specified, the parameter values in all figures are the "typical" ones mentioned in Table 1.

As can be seen from the series of images shown in Fig. 5b, third order filaments, similar to the 2nd order ones, start to form during the propagation through the taper. However, instead of appearing as "shoulders" on the side of the light beam, they grow up on the “corners” of the "top hat" intensity distribution (this kind of filaments was noticed in Ref. [Lang 1993]), which typically, though not necessarily, emerges later than the 2nd order filaments. The mechanism of their formation is actually the same as of the 2nd order. As soon as a flat “top hat” is formed, the flow of photons towards the center is blocked due to the absence of the refractive index variation (see Fig. 7c). New photons arriving from the taper edge then build up a filament. According to this understanding, a "top-hat" intensity distribution inherently favors filamentation. The propagation angles of the 3rd order filaments are smaller than those of the 2nd order filaments. At very small taper angles, 3rd order filaments dominate because the beam rapidly develops a “top-hat” shape.

4. Conclusions

Three orders of filamentation have been discovered within the typical ranges of the parameters of tapered power amplifiers. First order filaments originate at the beginning of the taper and are not related to the taper edge. They are caused by small perturbations and the presence of unnecessary amplifying medium which lets these perturbations grow. First order filaments can be eliminated by choosing a small enough taper angle.

Second order filaments are not caused by perturbations; they are generated by the beam itself during its propagation and appear as “shoulders” in the intensity distribution. The reason for their

appearance is a mismatch between the optical intensity and the current density (and, consequently, the gain). In the situation considered in this work, this mismatch is caused by the taper edge. The mismatch necessitates a flow of photons from the edge of the taper towards its center. As soon as the flow is disrupted, a filament develops. The 2nd order filaments can be suppressed or sometimes even eliminated by "smoothing" the taper edge.

Third order filaments are produced by the beam when its intensity distribution develops a "top hat" shape. The reason for their formation is very similar to that of the 2nd order. Namely, the "top hat" prevents the photon flow towards the beam center. The photons coming from the sides pile up on the “corners” of the "top hat" and “bat-ears” start to grow. Very small taper angles encourage 3rd order filamentation by drawing the beam to a “top-hat” shape.

To achieve the highest brightness, the taper angle should be small enough to eliminate first order filamentation and large enough to avoid the promotion of the third order. Further, taper edge "smoothing" should be employed to prevent second order filamentation. Generally, it is desirable to match the current profile to the optical mode profile.

References

L. Borruel *et al.*, “Quasi-3D Simulation of High-Brightness Tapered Lasers,” IEEE J. Quantum Electr. **40**, 463 – 472 (2004a).

L. Borruel *et al.*, “Modeling of Patterned Contacts in Tapered Lasers,” IEEE J. Quantum Electr. **40**, 1384 – 1388 (2004b).

L. Borruel *et al.*, “Design strategies to increase the brightness of gain guided tapered lasers,” Opt. Quant. Electron. **40**, 175 – 189 (2008).

D. J. Bossert, G. C. Dente and M. L. Tilton, “Filamentation in high-power tapered semiconductor amplifiers,” *SPIE*, vol. **3001**, 63-73 (1997).

S.R. Chinn, P.S. Zory and A.R. Reisinger, "A model for GRIN-SCH-SQW diode lasers", IEEE J. Quantum Electr. **24**, 2191 – 2214 (1988).

L. A. Coldren and S. W. Corzine, *Diode Lasers and Photonic Integrated Circuits*, Wiley (1995).

S. Delépine *et al.*, “How to Launch 1 W Into Single-Mode Fiber From a Single 1.48-µm Flared Resonator,” IEEE J. Sel. Top. Quant. 7, 111 – 123 (2001).

G. C. Dente, “Low Confinement Factors for Suppressed Filaments in Semiconductor Lasers,” IEEE J. Quantum Electr. **37**, 1650 – 1653 (2001).

R. J. Lang, “Numerical Analysis of Flared Semiconductor Laser Amplifiers,” IEEE J. Quantum Electr. **29**, 2044 – 2051 (1993).

D. Mehuys, D. F. Welch, and L. Goldberg, “2.0 W CW diffraction-limited tapered amplifier with diode injection,” Electron. Lett. **28**, 1944 – 1946 (1992).

M. Mikulla, “Tapered High-Power, High-Brightness Diode Lasers: Design and Performance,” in R. Diehl (Ed.), *High-Power Diode Lasers*, Topics Appl. Phys. **78**, 265–288 (2000).

S. Sujecki *et al.*, “Nonlinear Properties of Tapered Laser Cavities,” IEEE J. Sel. Top. Quant. **9**, 823 – 834 (2003).

J. M. Tijero *et al.*, “Analysis of the performance of tapered semiconductor optical amplifiers: role of the taper angle,” Proceedings of the 14th International Conference on Numerical Simulation of Optoelectronic Devices, Palma de Mallorca, Spain (2014).

A. H. Paxton and G. C. Dente, “Filament formation in semiconductor laser gain regions,” J. Appl. Phys. **70**, 2921 – 2925 (1991).

B. Sumph, *et al.*, “High-brightness quantum well tapered lasers,” IEEE J. Sel. Top. Quant. **15**, 1009-1020 (2009).

J. N. Walpole *et al.*, “High-power strained-layer InGaAs/AIGaAs tapered traveling wave amplifier,” Appl. Phys. Lett. **61**, 740 – 742 (1992).

J. N. Walpole *et al.*, “Gaussian Patterned Contacts for Improved Beam Stability of 1.55-µm Tapered Lasers,” IEEE Photonic Tech. L. **12**, 257 – 259 (2000).

H. Wenzel, G. Erbert and P.M. Enders, "Improved Theory of the Refractive-Index Change in Quantum-Well Lasers", IEEE J. Sel. Top. Quant. **5**, 637 – 642 (1999).

J. K. White, J. G. McInerney and J. V. Moloney, “Effects of the injection current profile shape on sidelobes in large-aperture semiconductor laser amplifiers,” Opt. Lett. **20**, 593 – 595 (1995a).

J. K. White, J. G. McInerney and J. V. Moloney, “Formation of sharply peaked sidelobes in large aperture single-pass semiconductor laser amplifiers,” Electron. Lett. **31**, 38 – 39 (1995b).